Acta Biomaterialia xxx (xxxx) xxx

Contents lists available at ScienceDirect

Acta Biomaterialia

journal homepage: www.elsevier.com/locate/actbio

Directionalities of magnetic fields and topographic scaffolds synergise to enhance MSC chondrogenesis

Cenk Celik[a], Alfredo Franco-Obregón[b,c,d,e,*], Eng Hin Lee[a,f], James HP Hui[a,f], Zheng Yang[a,f,*]

[a] Department of Orthopaedic Surgery, Yong Loo Lin School of Medicine, National University of Singapore, Singapore 119228
[b] Department of Surgery, Yong Loo Lin School of Medicine, National University of Singapore, Singapore, 119228
[c] BioIonic Currents Electromagnetic Pulsing Systems Laboratory, BICEPS, National University of Singapore, Singapore, 117599
[d] Institute for Health Innovation & Technology, iHealthtech, National University of Singapore, Singapore, 117599
[e] Department of Physiology, Yong Loo Lin School of Medicine, National University of Singapore, DSO (Kent Ridge) Building, #04-01, 27 Medical Drive, Singapore, 117593
[f] Tissue Engineering Program (NUSTEP), Life Sciences Institute, National University of Singapore, DSO (Kent Ridge) Building, #04-01, 27 Medical Drive, Singapore, 117510

ARTICLE INFO

Article history:
Received 21 August 2020
Revised 15 October 2020
Accepted 26 October 2020

Keywords:
Pulsed electromagnetic fields
mesenchymal stem cells
electrospun fibres
chondrogenesis
mechanotransduction

ABSTRACT

Mesenchymal stem cell (MSC) chondrogenesis is modulated by diverse biophysical cues. We have previously shown that brief, low-amplitude pulsed electromagnetic fields (PEMFs) differentially enhance MSC chondrogenesis in scaffold-free pellet cultures versus conventional tissue culture plastic (TCP), indicating an interplay between magnetism and micromechanical environment. Here, we examined the influence of PEMF directionality over the chondrogenic differentiation of MSCs laden on electrospun fibrous scaffolds of either random (RND) or aligned (ALN) orientations. Correlating MSCs' chondrogenic outcome to pFAK activation and YAP localisation, MSCs on the RND scaffolds experienced the least amount of resting mechanical stress and underwent greatest chondrogenic differentiation in response to brief PEMF exposure (10 min at 1 mT) perpendicular to the dominant plane of the scaffolds (Z-directed). By contrast, in MSC-impregnated RND scaffolds, greatest mitochondrial respiration resulted from X-directed PEMF exposure (parallel to the scaffold plane), and was associated with curtailed chondrogenesis. MSCs on TCP or the ALN scaffolds exhibited greater resting mechanical stress and accordingly, were unresponsive, or negatively responsive, to PEMF exposure from all directions. The efficacy of PEMF-induced MSC chondrogenesis is hence regulated in a multifaceted manner involving focal adhesion dynamics, as well as mitochondrial responses, culminating in a final cellular response. The combined contributions of micromechanical environment and magnetic field orientation hence will need to be considered when designing magnetic exposure paradigms.

1. Introduction

Mesenchymal stem cells (MSCs) exhibit multipotency to differentiate into multiple cell lineages including osteoblasts, adipocytes, chondrocytes and myocytes [1,2]. Preclinical studies have demonstrated promising therapeutic applications for MSCs in cell-based strategies to repair or replace damaged or lost cells and tissues, including articular cartilage [3–5]. MSC-derived cartilage conventionally has been shown to largely consist of fibrocartilage, interspersed with insubstantial amounts of hyaline cartilage and thereby functionally lacking the biochemical composition and mechanical strength of native cartilage [6,7]. Innovations are thus needed to improve the functionality of MSC-based cartilage regeneration.

Studies have examined the interaction between stem cells and different microenvironmental cues presented on functionalised scaffolds [8], as well as the efficacies of different stimulation protocols [9,10] in inducing MSC-based cartilage regeneration. Substrate-mediated and other forms of biophysical stimulation have been shown to influence cellular function through the recruitment of enzymatic cascades in common with mechanotransduction that ultimately impact cell fate decisions [11–13]. ECM-binding by cells is assisted by membrane-embedded integrin receptors that convey mechanical signals internally from the cell periphery through

* Corresponding authors
E-mail addresses: suraf@nus.edu.sg (A. Franco-Obregón), dosyz@nus.edu.sg (Z. Yang).

https://doi.org/10.1016/j.actbio.2020.10.039
1742-7061/

the focal adhesion complexes (FAs) and associated cytoskeletal elements, triggering intracellular signalling cascades that are ultimately transmitted to the transcriptional machinery within the nucleus of the cell [14]. Mechanotransduction within the cell is dependent on FA and cytoskeleton actin dynamics regulated by tyrosine (FAK) [15–17] and serine-threonine kinases (MAPK) [18] as well as the transcriptional level (YAP/TAZ) [19,20], concomitantly have been implicated in chondrogenic progression [21,22].

We have previously demonstrated that brief exposure to PEMFs (10 minutes), applied once during early chondrogenic induction, were most efficacious at promoting MSC chondrogenesis in pellet cultures [23], whereby the exposure parameters were established by targeting the developmental expression of certain Transient Receptor Potential (TRP) channels previously implicated in chondrogenic induction and hence, unique in strategy and structure from other magnetic exposure paradigms [23–25]. Nonetheless, despite the fact that investigations examining the effects of PEMFs over MSC chondrogenesis have traditionally focused on scaffold-free pellet cultures [23,26–28], this platform lacks translational practicality for cell delivery, particularly for critically-sized cartilage lesions. Here, MSCs were seeded onto randomly-oriented or aligned electrospun scaffolds, subjecting the laden cells to distinctive mechanical environments. MSC response to directional mechanical stress is dependent on orientation of the cell traction force, such as that generated on aligned fibres that ultimately influence fibrochondrogenic differentiation [29,30]. Here, we further examined the influence of directionally applied PEMFs on the chondrogenic differentiation of MSCs laden onto topographically-variant fibrous scaffolds. The objective was to investigate the interactions between basal mechanotransduction, substrate-mediated cellular alignment and PEMF directionality over chondrogenic induction and to elucidate the underlying mechanisms and intracellular signalling pathways elicited by the coupling of mechano-conditioning and pulsed magnetic field direction.

2. Materials and Methods

2.1. Fabrication and characterisation of electrospun fibrous scaffolds

Poly(lacto-co-caprolactone) (PLCL, PURASORB PLC 7015, Corbion, the Netherlands) was dissolved in 1,1,1,3,3,3-Hexafluoro-2-propanol (HFIP, Sigma-Aldrich, Germany) to form a 10% PLCL/HFIP solution. Electrospun scaffolds were manufactured using a custom-made rotating mandrel collector (Cintechco Technologies, Singapore). Briefly, PLCL/HFIP solution was supplied to the electrospinning system at a speed of 1 ml/h with a voltage supply of 15 kV. Randomly-oriented (RND) and parallel aligned fibres (ALN) were fabricated with the rotating collector set at 300 and 3000 rpm, respectively. Scanning electron micrographs were taken using a JEOL FEG-SEM instrument (JSM-6701F, Massachusetts, USA). The fibre orientation and porosity of the scaffolds were measured using ImageJ software (National Institutes of Health, Maryland, USA). Uniaxial tensile strength of the scaffolds was conducted by Instron Model 5543 Pull Tester (Massachusetts, USA). Aligned scaffolds were tested for both in parallel (Y) and perpendicular (X) fibre orientations in relation to tensile force direction. The scaffolds were kept in a dehumidified box until cell culture studies.

2.2. Human bone marrow-derived MSC culture

Human bone marrow mesenchymal stem cells (MSCs) were purchased from RoosterBio, Inc. (Maryland, USA) at passage 3. MSCs were further expanded in RoosterBasal™ Protein Free medium supplemented with RoosterBio Media Booster in a humidified, 5% CO_2 atmosphere at 37°C. MSCs at passage 5 were used for studies.

Table 1
Nomenclature of test groups.

Topography	PEMF amplitude (mT)	PEMF direction	Plot abbreviation
Tissue culture plastic (TCP)	0	N/A	NP
	1	Z	Z
	1	X	X
Randomly-oriented fibres (RND)	0	N/A	NP
	1	Z	Z
	1	X	X
Aligned fibres (ALN)	0	N/A	NP
	1	Z	Z
	1	X	X
	1	Y	Y

N/A: not applicable, **mT**: milliTesla; **NP**: no PEMFs

2.3. MSC chondrogenic differentiation

Chondrogenic differentiation of MSCs was induced three days after seeding the MSCs onto three different topographies, namely, polystyrene tissue culture plastic (TCP; Cellstar® 24-well multiwell plates, Greiner Bio-one), randomly-oriented (RND) and aligned (ALN) PLCL electrospun scaffolds. As MSCs on TCP and fibrous scaffolds have drastically different proliferation rate, cell seeding on TCP versus fibrous scaffolds was adjusted accordingly to ensure that MSCs reached similar cell-cell contact at the time of PEMF and chondrogenic induction. Briefly, cells were seeded at a density of 4 x10^3 cells/ml onto TCP and 60 x10^3 cells/ml onto fibrous scaffolds to obtain similar cell confluence at the day of chondrogenic induction. Cells were allowed for attachment and proliferation in expansion medium. Chondrogenic differentiation was induced in medium comprised of high glucose DMEM (Gibco, Thermo Fischer Scientific, Massachusetts, USA) supplemented with 4 mM proline, 50 µg/ml ascorbic acid, 1% ITS-Premix (Becton-Dickinson, San Jose, USA), 1 mM sodium pyruvate, 10^{-7} M dexamethasone (Sigma-Aldrich, St Louis, USA) and 10 ng/ml transforming growth factor-β3 (TGF-β3; R&D Systems, Minneapolis, USA) without antibiotic supplementation, for 14 days or 21 days. To study the involvement of focal adhesion kinase (FAK) FAK inhibitor, PF-573228 (20 µM; PZ0117, Sigma-Aldrich) was added to chondrogenic media 1 h before PEMF treatment and removed 1 h after PEMF treatment.

2.4. PEMF exposure paradigm

The PEMF delivery device used in this study has been previously described [23,31,32]. MSCs on TCP, RND and ALN scaffolds were first subjected to single exposures ranging from 0 - 3 mT for 10 min administered in Z direction. Using the topography on which MSCs were most responsive to PEMFs, i.e. the RND scaffolds, the effect of magnetic field duration and efficacy of multiple exposures on MSC chondrogenic differentiation was further determined. Briefly, MSCs on the RND scaffolds were subjected to either 5, 10, 20 or 30 min of PEMF exposures once, or single (Day 1), double (Day 1 and 2) or triple exposures (Day 1, 2 and 4). For directionality experiments, MSCs on different topographies were subjected to PEMFs, applied in different directions, as shown in Figure 1. Briefly, MSCs in chondrogenic differentiation medium were exposed for 10 min to PEMFs at an amplitude of 1 mT, administered in either the Z or X directions - perpendicular (field lines directed upward) or parallel to the X-Y (culture dish) plane, respectively. As the cell alignment on ALN scaffolds was in the Y direction, Y-directed PEMFs were applied parallel to the long axis of embedded MSCs. The nomenclature of the studied groups is listed in Table 1.

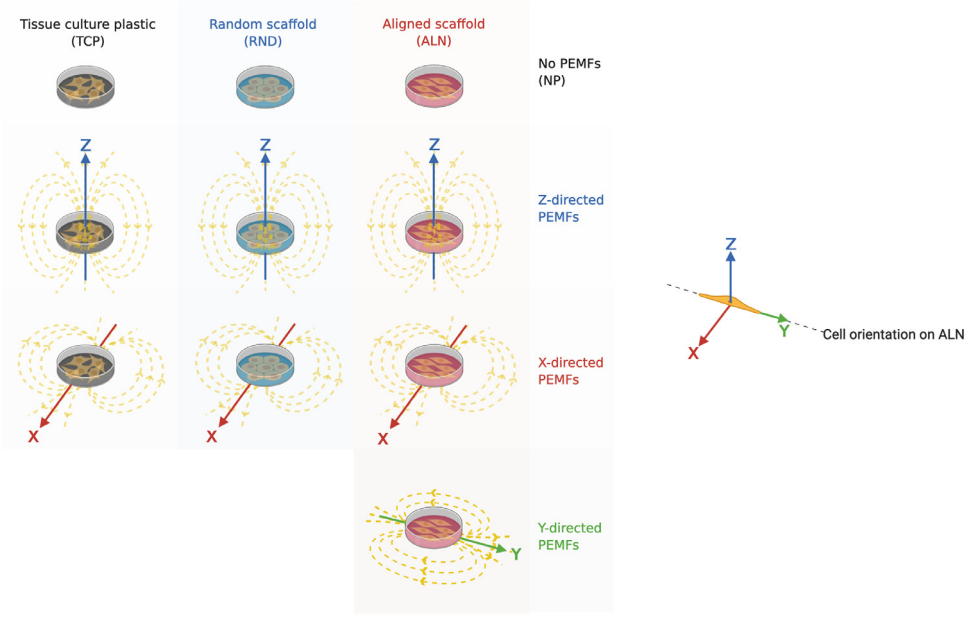

Fig. 1. Magnetic field direction in relation to cell alignment.

2.5. Cell apoptosis

Caspase-3/7 activity was measured using the Caspase-Glo® 3/7 Assay kit (Promega, Madison, USA). Briefly, the add-mix-measure reagent was added to MSC-seeded topographies at room temperature and then was shaken at 400 rpm for 30 s, followed by a 30-min of incubation at room temperature. The apoptosis assay was carried out at Day 1 and Day 3 of differentiation following PEMF exposure.

2.6. Cell proliferation

Cell viability was evaluated with alamarBlue® Cell Proliferation assay (Bio-Rad) according to the manufacturer's protocol. Briefly, 10x alamarBlue® was diluted to 1:10 ratio in the cell culture medium, and the diluted dye was added to each test group and incubated in the dark, humidified 5% CO_2 atmosphere at 37°C for 2 h. Fluorescent readings were obtained by a spectrophotometer (Tecan i-Control Infinite 200 plate reader, Switzerland) at wavelengths of 570 nm and 600 nm at day 1, 3, 5 and 7. Duplicates of triplicate for each test group were measured and averaged before subtracting blank. alamarBlue® reduction percentile was calculated by the manufacturer's reduction conversion formula.

2.7. Real-time PCR analyses

Total mRNA was extracted using the TRIzol® Reagent (Thermo Fischer Scientific) and purified using RNeasy® Mini Kit (Qiagen, Germany). Reverse transcription was conducted using the iScript™ cDNA synthesis kit (Bio-Rad, USA) with a 100-ng total RNA. Real-time PCR was performed on StepOnePlus™ Fast Real-time PCR System (Applied Biosystems, USA) with Tera-Cybr 2x Master Mix (SGenix, Singapore) with the primers set in Supplementary Table 1 at 95°C for 10 s and 40 cycles of amplification, which consisted of denaturation step at 95°C for 30 s, and extension step at 60°C for 30 s. The gene expression level normalised to glyceraldehyde-3-phosphate dehydrogenase (*GAPDH*) was calculated using the $2^{-\Delta\Delta Ct}$ formula with reference to the undifferentiated MSCs.

2.8. Immunofluorescence staining

Cells were fixed in 10% neutral-buffered formalin solution (Sigma-Aldrich), permeabilised with Triton X-100 (0.1%, Sigma-Aldrich), followed by blocking in Ultra V Block (Thermo Scientific). Samples were treated with antibodies for ECM proteins; COL II (Clone 6B3; Chemicon Inc.), COL I (Clone C245B, Sigma-Aldrich) and Aggrecan (AlexaFluor® 647-conjugated anti-mouse aggrecan, Santa Cruz Biotechnology), or cytoskeletal proteins pFAK (ab81298, Abcam, Cambridge, UK) and YAP (sc-101199, Santa Cruz Biotechnology, CA, USA), followed by AlexaFluor® 594 or 488 secondary antibodies (Invitrogen), respectively. F-actin was stained with TRITC-conjugated phalloidin (Invitrogen). Nuclei were counter-stained with 4',6-diamidino-2-phenylindole (SlowFade™ Gold Antifade Mountant with DAPI, Thermo Fischer Scientific). The samples were then visualised with an Olympus IX81 motorised inverted microscope system (Olympus, Japan). Fluorescence intensity of the ECM proteins or the number and length of FAK, and YAP localisation were semi-quantified by a self-developed algorithm in ImageJ on 15 image fields per test group [33]. The nucleus and cell circularity were evaluated using images of the nucleus- and f-actin-stained cells. Circularity was presented as numbers between 0 and 1, where 1 is the perfect circle.

2.9. Western blotting

Cells were harvested 1 h following PEMF exposure and lysed by M-PER® Mammalian Protein Extraction Reagent (Thermo Scientific) supplemented with Pierce™ Protease and Phosphatase Inhibitor (Thermo Scientific). Protein concentration was determined using Pierce™ bicinchoninic acid (BCA) Protein Assay Kit (Thermo Scientific). Twenty µg of protein samples were mixed with Laemmli protein sample buffer (Bio-Rad), denatured at 95°C for 10 min, and electroporated on a 12% Mini-PROTEAN® TGX™ precast gels (Bio-Rad). The separated proteins were then transferred to a nitrocellulose membrane (0.45 µm, Bio-Rad) and incubated with anti-β-actin antibody (ab8226, Abcam), mouse anti-FAK antibody (ab72140, Abcam), rabbit anti-FAK (phospho Y576 + Y577; ab76244, Abcam), mouse anti-ERK1 + ERK2 antibody (ab54230, Abcam), rabbit anti-ERK1 (phospho T202) + ERK2 (phospho T185)

antibody (ab76244, Abcam), mouse anti-P38 antibody (ab31828, Abcam), rabbit anti-P38 (phospho T180 + Y182) antibody (ab4822, Abcam) and mouse anti-YAP (63.7) antibody (sc-101199, Santa Cruz Biotechnology). Blots were incubated in horseradish peroxidase (HRP)-conjugated anti-mouse (ab97023, Abcam) or anti-rabbit secondary antibodies (ab6721, Abcam). The protein bands were detected with SuperSignal® West Dura Extended Duration Substrate chemiluminescence kit (Thermo Scientific) and visualised via the ChemiDoc^{TM} MP Imaging System (Bio-Rad).

2.10. Mitochondrial Stress Measurements

Effects of PEMFs on mitochondrial stress was assessed by the Mitochondrial Stress Test Complete Assay Kit (ab232857, Abcam). Briefly, 6 x10^3 cells/well were seeded onto scaffolds, placed in a 96-well plate, followed by overnight incubation for cell attachment. Next, the chondrogenic medium was introduced two hours before PEMF exposure. 1.5 µM of Oligomycin, 2.5 µM of Carbonyl cyanide-4-phenylhydrazone (FCCP) and 1.0 µM of Antimycin A were separately supplemented into the media, containing extracellular O_2 probe, immediately post-pulse. The samples were then sealed using prewarmed HS mineral oil. The fluorescence measurement was carried out for excitation and emission at the wavelengths of 340 nm and 655 nm, respectively, by FLUOstar Plate Reader (BMG) using time-resolved fluorescence mode at 37°C for about 1.1 hours. Briefly, multichromatic integration times were set to 30/70 µs for excitation filter and 30/30µs for emission filter for about 30 cycles with a cycle time of 60 sec. The fluorescence data were then converted to lifetime values (µs) according to the kit manufacturer's formula, and the slopes from the plots of drug-treated samples (Oligomycin, FCCP and Antimycin A) and untreated samples were calculated by linear regression ($R^2 > 0.99$). Using formulae provided by the kit manufacturer, the basal respiration, the non-ATP-coupled O_2 consumption, the ATP-coupled O_2 consumption, the spare respiratory capacity and the maximal respiration were calculated for the evaluation of mitochondrial stress.

2.11. Statistical Analysis

All experiments were performed in biological replicates (n = 3). Statistical analyses were assessed by *Student's* t-test for comparison of PEMF directions within a topography; whereas ordinary one-way ANOVA was used for multiple comparisons across different topographies in GraphPad Prism 8 software. Statistical significance for all data was set at $p < 0.05$. All data are presented as mean ± SD of triplicates from at least two independent experiments unless specified otherwise.

3. Results

3.1. Characterisation of electrospun scaffolds

SEM images (Fig. 2A) showed the distinct nanofibrillar organisations present in the random (RND) and aligned (ALN) scaffolds (Fig. 2B). RND and ALN nanofibers had comparable fibre diameters (Fig. 2C; 0.6 µm ± 0.02, p = 0.3909) and porosities (Fig. 2D; 75.31% ± 1.51, p = 0.0684). Uniaxial tensile testing also showed that RND and ALN scaffolds had similar *Young's* moduli (Fig. 2E) and tensile strengths (Fig. 2F) when measured in the longitudinal (Y-direction) plane to fibre alignment (4.3 MPa ± 0.21, p = 0.9980). By contrast, tensile force (X-direction) applied perpendicular to the ALN scaffolds resulted in collapse of the scaffold ($p < 0.05$) (Fig. 2E-F). Apparent differences in *Young's* moduli and strength when forces were applied longitudinally (Y) versus perpendicularly (X) to fibre alignment reflected uniformity of fibre orientation within the ALN scaffolds. MSCs adopted distinct morphologies between the different scaffolds (Fig. 2G) and achieved similar confluencies at the time of chondrogenic induction and PEMF exposure under our seeding protocol (Fig. 2H).

3.2. Optimisation of PEMF conditions for MSC chondrogenesis on fibrous scaffolds

MSCs seeded onto TCP, RND or ALN scaffolds were subjected to Z-directed PEMFs, ranging from 1 - 3 mT for 10 min on the first day of chondrogenic induction (see Fig. 2H for cell confluency); a non-exposed group (NP) handled identically served as controls. MSCs on TCP underwent limited chondrogenesis and exhibited modest upregulations of *COL II* and *ACAN* in response to exposure at 2 mT PEMFs (Fig. 3A). By contrast, MSC chondrogenesis on the RND scaffolds was dramatically augmented by exposure to 1 mT PEMFs, associated with upregulations of *SOX9, COL II* and *ACAN* expression by 1.61-, 38.4- and 4.55-fold, respectively, whereas exposure to 2 and 3 mT did not induce significant changes in chondrogenic markers (p = 0.9578). A more modest and limited enhancement of MSC chondrogenesis was observed on the ALN scaffolds with only *COL II* expression showing an enhancement following exposures at 1 and 2 mT (< 30-fold), albeit at a 19-fold lower level compared to that induced on the RND scaffolds upon 1 mT exposure for 10 min.

We investigated the consequences of repetitive PEMF exposures over MSC chondrogenesis on the RND scaffolds (Fig. 3B). PEMFs at 1 mT were administered once (day 1), twice (days 1 and 2) or thrice (day 1, 2 and 4) following chondrogenic induction to ascertain potential dosing effects. A single PEMF exposure (1x) applied at the initiation of chondrogenesis was the most effective at enhancing chondrogenesis. Multiple PEMF exposures either resulted in inhibition of chondrogenesis or rendered no additional enhancement. MSCs on the RND scaffolds were also exposed to 1 mT PEMFs in the Z direction for 5, 10, 20 or 30 min. Brief exposures of only 10 minutes gave the greatest chondrogenic induction, reflected by increased expressions of *SOX9, COL II, ACAN* (Fig. 3C); shorter or longer exposures gave weaker responses. From here onwards, administered PEMF exposures were at 1 mT amplitude, applied once for 10 min, on the first day of chondrogenic induction and compared to non-exposed counterparts, unless otherwise noted.

3.3. Effect of directional PEMF on MSC chondrogenesis

After defining a reference PEMF efficacy window, the chondrogenic consequences of directional PEMFs and surface topography were examined (Fig. 1). Z-directed PEMFs resulted in elevated transcript levels of *SOX9, COL II* and *ACAN* when applied to MSCs on the RND scaffolds, but not when applied to MSCs on TCP or ALN scaffolds (Fig. 4A). By contrast, X-directed PEMFs either reduced or had no effect over the expressions of these same chondrogenic markers when applied to MSCs on the RND scaffolds/TCP and ALN scaffolds, respectively. Notably, Y-directed PEMFs applied to the ALN scaffolds, parallel to the longitudinal orientation of the cells, demonstrated strong inhibition. Accordingly, the ratios of *COL I* and *COL X* to *COL II*, indicators for the fibroblastic and hypertrophic phenotypes, respectively, were uniformly decreased and increased by Z- and X-directed PEMFs, respectively, when applied to MSCs of RND scaffolds. Unexpectedly, the ratio of *COL X*/*COL II* was increased by X-directed, but not Y-directed, PEMFs for MSCs on the ALN scaffolds.

Immunofluorescence staining for COL II, ACAN and COL I at 21-days following PEMF exposure demonstrated significantly enhanced depositions of COL II and ACAN in response to Z-directed PEMFs delivered to MSCs on the RND scaffolds, compared to when PEMF delivery was in the X direction or in non-exposed cells

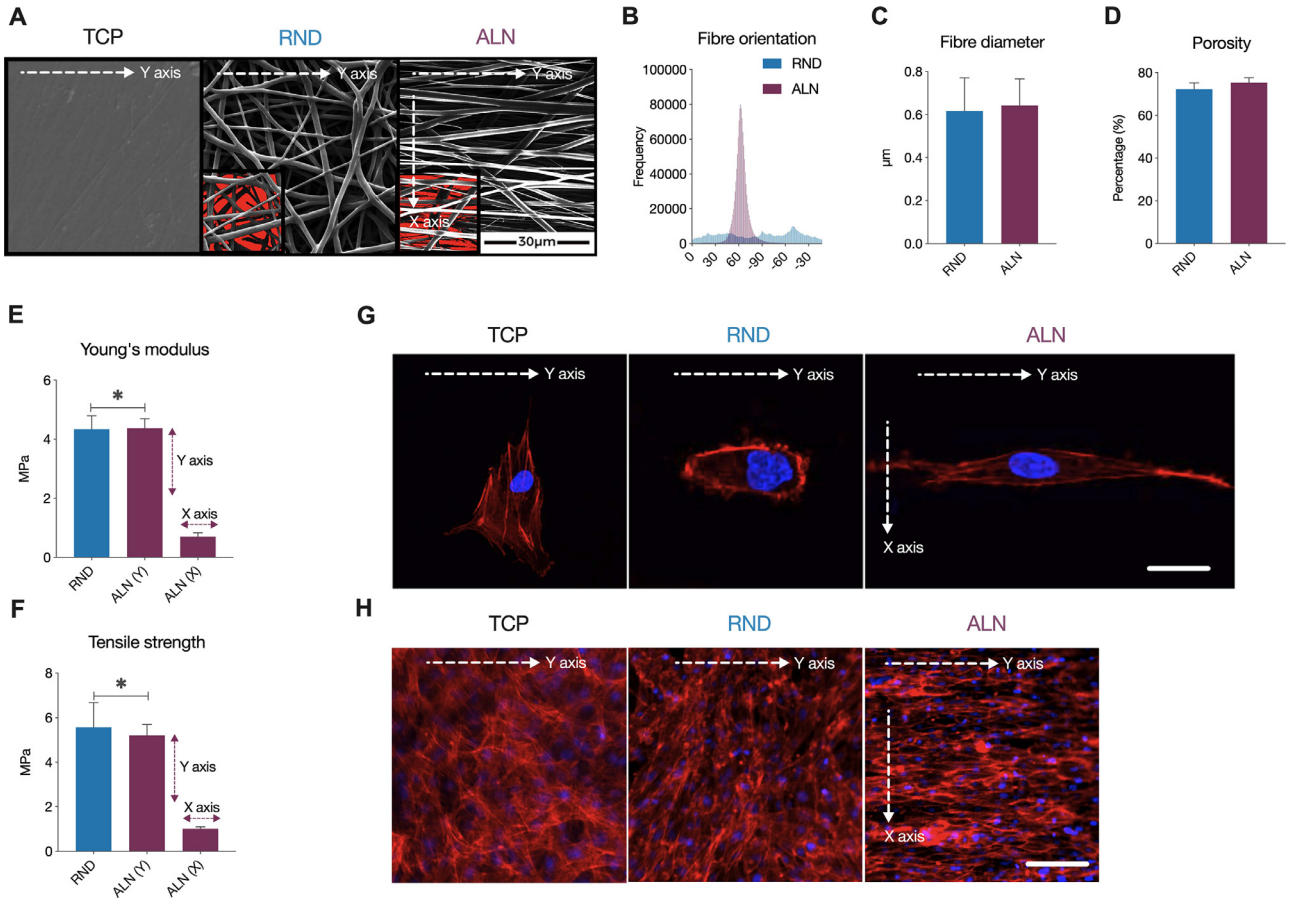

Fig. 2. Structural and mechanical characterisation of electrospun scaffolds. **(A)** SEM micrographs. Segments presented as red indicates pores within the fibres. Scale bar applies to images of all three topographies. **(B)** Fibre orientation analysis, **(C)** fibre diameter, **(D)** porosity, **(E)** elasticity (*Young's*) moduli and **(F)** tensile strengths of the RND and ALN scaffolds. Data shown represent means ± SD, n = 5. * denotes significance of $p < 0.05$ compared to the perpendicular force applied on ALN (P). Red arrows indicate the direction of the force on ALN scaffolds. **(G)** MSC cell morphology on TCP, RND and ALN scaffolds. Scale bar represents 10 μm and applies to all images **(H)** Cell confluency on TCP, RND and ALN scaffolds at the day of chondrogenic induction. Scale bar represents 20 μm and applies to all images (red ≡ f-actin; blue ≡ nucleus).

(Fig. 4B), reiterating that Z-directed PEMFs exert a clear chondrogenic effect over MSCs on RND scaffolds. Interestingly, COL I deposition was strongly reduced by X-directed PEMFs delivered to MSCs on the RND scaffolds. On the other hand, PEMFs of any directionality were largely ineffective over the weak ECM deposition from MSCs on ALN scaffolds. These results indicate that Z- and X-directed PEMFs (1 mT) bias chondrogenesis towards hyaline-like or hypertrophic phenotypes, respectively, in MSCs on RND scaffolds.

3.4. Effects of directional PEMFs on MSC proliferation and viability

The effects of directional PEMF exposure over MSC apoptosis on TCP, RND and ALN scaffolds were analysed. Caspase-3/7 activity increased over three days for MSCs on TCP under all conditions and was further augmented by X-directed PEMFs relative to non-exposed counterparts (NP controls) (Fig. 3D), indicating increased apoptosis. By contrast, MSCs on the RND scaffolds exhibited overall lower levels of basal apoptosis that were unaffected by PEMF exposure of any orientation. Apoptosis was initially lowest for MSCs on the ALN scaffolds and was further inhibited by PEMFs in the plane of the dish (Y- and X-directed PEMFs) at day 3 but augmented by Z-directed PEMFs at day 1. Apoptotic and proliferative responses largely paralleled each other (Fig. 3E). MSCs on either scaffold exhibited overall lower proliferation rates relative to TCP and Z-directed PEMFs had little consequence on proliferation regardless of scaffold nature. By contrast, PEMFs applied in the plane of the dish either in the X- or Y-directions further depressed MSC proliferation on both the RND and ALN scaffolds. Changes in apoptosis following PEMF exposure were hence correlated with mitochondrial-induced proliferation [34] subject to modulation by analogous magnetic fields [31].

3.5. Dynamic effects of directional PEMFs on cell morphology

Changes in MSC morphology, indicative of mechanical force distribution, were monitored on TCP, RND and ALN scaffolds immediately before PEMF (bP), immediately post-PEMF (iPP), 1-hour post-PEMF (1hPP) and 1-day post-PEMF (1dPP) exposure (Fig. 5A). MSC morphology on the RND scaffolds was more spherical than on TCP or the ALN scaffolds (Fig. 5C). Notably, cell body circularity further increased iPP and 1hPP for MSCs on the RND scaffolds following Z-directed PEMF exposure, reverting to normal by 1dPP, whereas X-directed PEMFs exerted no change. On the other hand, for MSCs on TCP and the ALN scaffolds, cellular circularities were largely unaffected by PEMF treatment regardless of directionality.

3.6. Effects of directional PEMF on focal adhesion kinase

The response of MSCs to PEMF orientation and substrate was examined at the level of focal adhesion assembly (Fig. 5B, D-E, F-G) and cytoskeletal organisation (Fig. 5B). MSCs on TCP were characterised by polygonal morphologies with randomly oriented lamellar cytoplasmic protrusions, peripheral and perinuclear pFAK distributions (Fig. 5B) and prominent stress fibre networks (Fig. 5A).

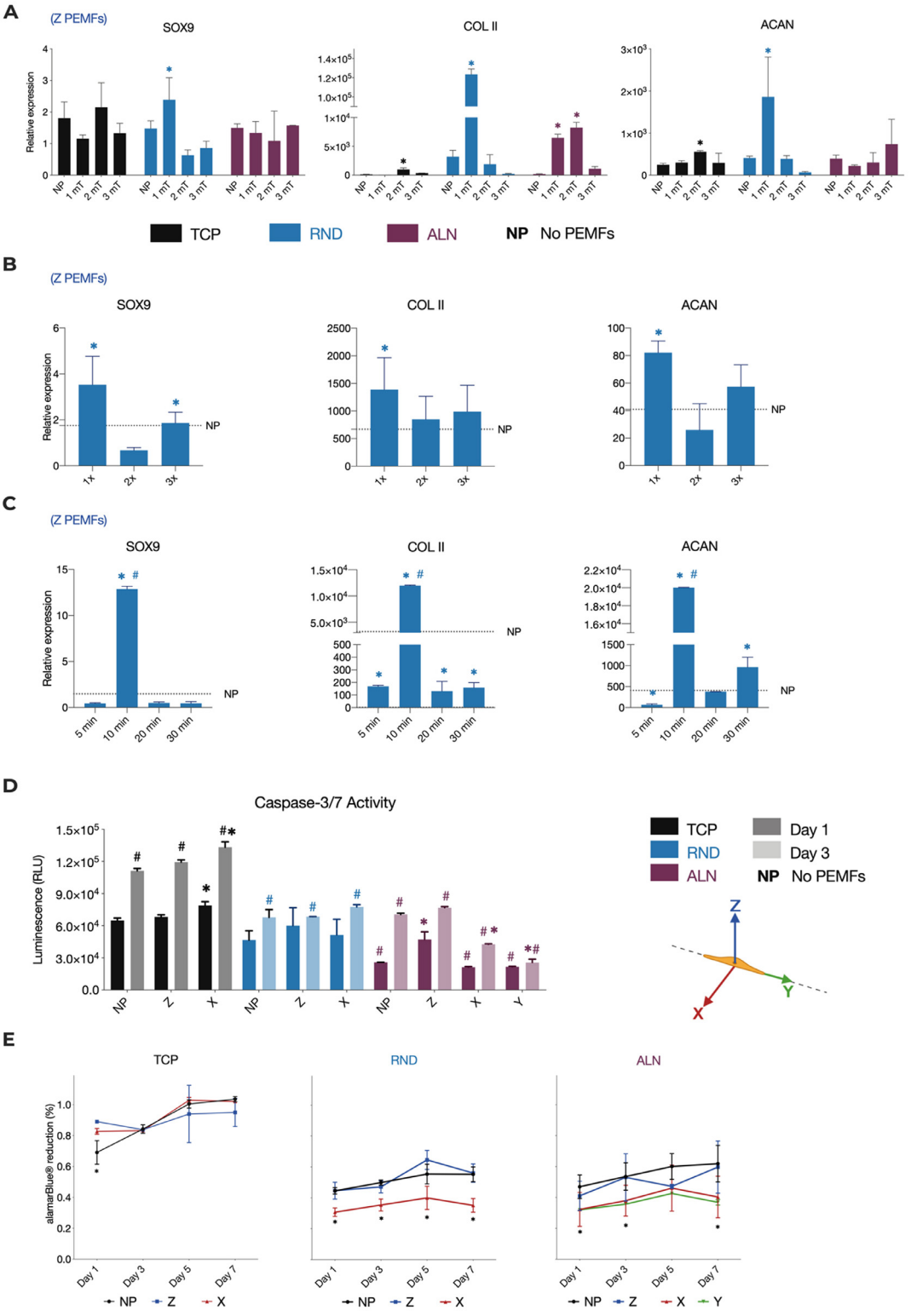

Fig. 3. Optimisation of PEMFs on the different surface topographies. **(A)** Relative expression of chondrogenic markers on TCP, RND and ALN in response to PEMF exposure. MSCs on the different topographies were subjected to a 10 min pulse, ranging from 1 – 3 mT, on the day of chondrogenic induction. **(B)** MSCs on RND were subjected to a single pulse of 1 mT at Day 1 (x) or multiple pulses on either Day 1 and 2 (2x) or Day 1, 2 and 4 (3x). **(C)** MSCs on RND were subjected to a single pulse of 1 mT with differing durations of 5, 10, 20 and 30 min, on the first day of chondrogenic induction. Cartilaginous markers' expressions at Day 14 were normalised to *GAPDH* and presented as fold change relative to levels in undifferentiated MSCs. **(D)** Caspase 3/7 activity measured by luminescence at Day 1 and Day 3 following PEMF exposure. Darker colours represent luminescence levels at Day 1 whereas lighter shades of respective colour represent luminescence levels at Day 3. **(E)** alamarBlue® reduction measured at Day 1, 3, 5 and 7 following PEMF exposure, when PEMFs administered only once at different directions on the day of chondrogenic induction. Z, X and Y coordinates represent PEMF exposure direction; NP denotes no PEMFs. * denotes significant change compared to non-exposed of respective topography at the same time point, whereas # denotes a significant decrease compared to non-exposed TCP control of respective time point ($p < 0.05$). Data shown represent means ± SD, n = 6 from 2 independent experiments.

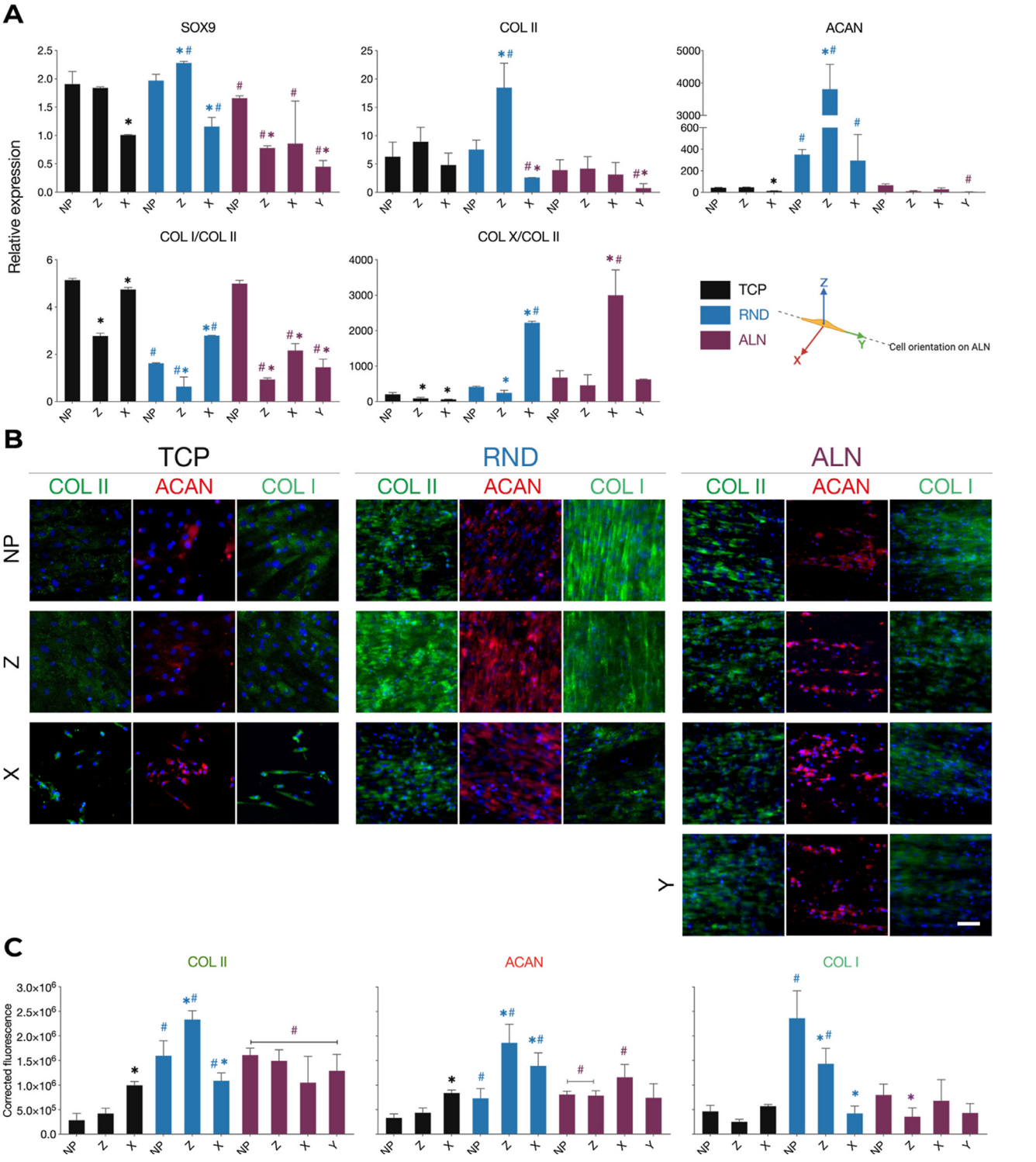

Fig. 4. Effect of directional PEMF on MSC chondrogenesis on different topographies. **(A)** Real-time PCR analysis of cartilaginous, fibroblastic and hypertrophic markers' expression after 14 days of differentiation, normalised to *GAPDH* and presented as fold change relative to levels in undifferentiated MSCs. Expressions of *COL I* and *COL X* were presented as a ratio to *COL II* expression. Data shown represent means ± SD, n = 6 from 2 independent experiments. **(B)** Immunofluorescent staining for COL II, ACAN and COL I deposition on TCP, RND and ALN in response to PEMFs at Day 21 of differentiation. Scale bar represents 20 μm and applies to all images. **(C)** Bar graphs represent semi-quantification of IFS. Data shown represent means ± SD, n = 15. * denotes significance level compared to the non-exposed TCP control. # denotes significance level compared to the non-exposed group of respective topography ($p < 0.05$). Z, X and Y coordinates represent PEMF exposure direction; NP denotes no PEMFs.

MSCs on the RND scaffolds retained polygonal morphology but were smaller in size and lacked prominent stress fibre networks, whereas MSCs on the ALN scaffolds were elongated, assuming the orientation of the scaffold fibre alignment, and exhibited parallelly aligned stress fibre networks (Fig. 5A). pFAK staining was discrete and uniformly-distributed in MSCs on both the RND and ALN scaffolds (Fig. 5B), although of overall greater density on the RND scaffolds (Fig. 5D). Developmentally, the number of pFAK complexes increased upon the administration of chondrogenic medium in MSCs on TCP and was further accelerated by Z-directed, but not by

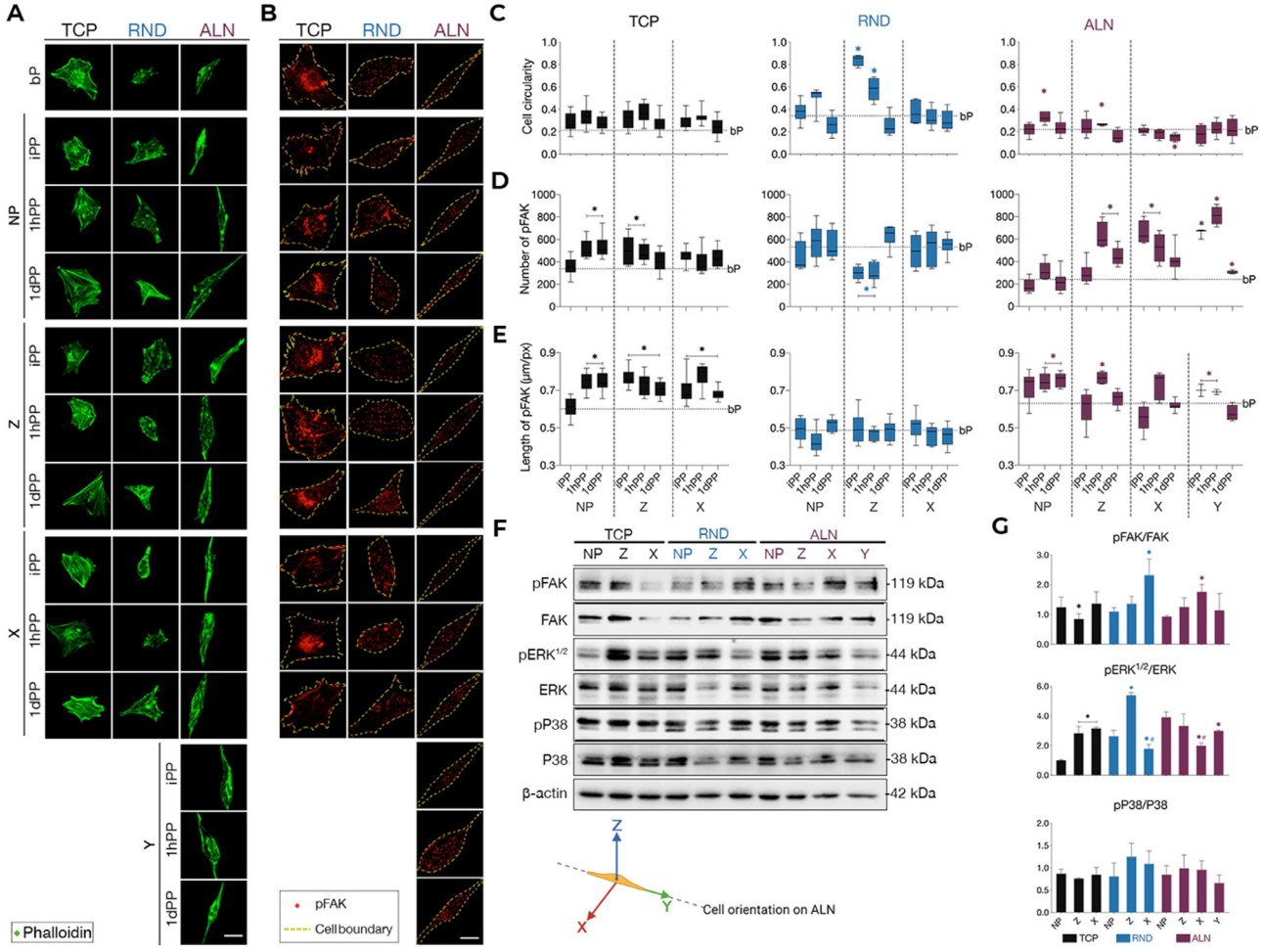

Fig. 5. Transient effects of directional PEMFs on pFAK in MSCs laden on TCP, RND and ALN. **(A)** Cell morphology under different conditions (green ≡ phalloidin). **(B)** pFAK probing by IFS (red ≡ pFAK; yellow dashes ≡ cell boundary). Scale bar represents 10 μm and applies to all images. Semi quantification of **(C)** cell circularity, **(D)** number of pFAK and **(E)** length of pFAK at bP, iPP, 1hPP and 1dPP. Data shown represent means ± SD, n = 15. **(F)** Western blot analysis for the effect of directional PEMFs on the activation of FAK, ERK and P38 expression in MSCs on different topographies at 1hPP. **(G)** Semi-quantification of phosphorylated FAK, ERK and P38 levels. Data shown represent means ± SD, n = 3 from 3 independent experiments. * denotes significance compared to the non-exposed group of the respective topography ($p < 0.05$). Z, X and Y coordinates represent PEMF exposure direction; NP denotes no PEMFs.

X-directed PEMFs. Notably, MSCs on RND scaffolds demonstrated an immediate reduction in the number of pFAK in response to Z-directed PEMF delivery that persisted 1-hour post-PEMF, whereas X-directed PEMFs did not induce a remarkable change. MSCs on the ALN scaffolds, on the other hand, demonstrated a generalised transient increase in the number of pFAK-positive complexes with PEMF exposure that was most pronounced for Y-directed fields. Therefore, a generalisable inverse relationship was observed between pFAK assembly and chondrogenic induction. pFAK size and dimensions was also subject to modulation by field orientation. The pFAK staining observed in MSCs on TCP and the ALN scaffolds were most elongated, whereas those in MSCs on the RND scaffolds were more punctate, suggesting that MSCs on both the TCP and the ALN scaffolds were experiencing greater substrate-mediated tensions (Fig. 5E). pFAK elongation was generally accentuated by PEMF exposure to MSCs on TCP, whereas PEMF exposure to MSCs on the RND scaffolds did not influence pFAK length. By contrast, PEMF exposure consistently decreased pFAK length in MSCs on ALN scaffolds yet increased in overall number. pFAK-mediated mechanotransduction via the ERK and P38 signalling pathways [35–37] was investigated (Fig. 5F-G). FAK phosphorylation was reduced by Z-directed PEMFs for MSCs on TCP, whereas they exerted no effect on MSCs on either the RND or ALN scaffolds. By contrast, X-directed PEMFs increased FAK phosphorylation for MSCs on both the RND and ALN scaffolds, whereas they had no effect on MSCs on TCP. ERK phosphorylation was reduced by X-directed PEMFs on the RND and ALN scaffolds. Notably, PEMFs of either Z or X orientation induced a significant increase in ERK phosphorylation on TCP to comparable levels as that detected at baseline (non-exposed) on the RND and ALN scaffolds. Overall, ERK phosphorylation was activated by: **(1)** all PEMFs on TCP; **(2)** Z-directed PEMFs on the RND scaffolds and; **(3)** not activated by Z-directed PEMFs on ALN scaffolds. By contrast, ERK phosphorylation was inhibited by: **(1)** X-directed PEMFs on RND scaffolds and; **(2)** X- and Y-directed PEMFs on ALN scaffolds. pP38/P38 level was not affected in all treatment groups.

3.7. Dynamic effects of directional PEMFs on YAP expression

YAP, a mechanosensitive transcriptional co-activator [38,39], exhibited predominantly cytoplasmic localisation in MSCs on the RND scaffolds, whereas greater nuclear localisation was detected in MSCs on TCP and the ALN scaffolds (Fig. 6A), agreeing with previous data indicating that rounded MSCs on the RND scaffolds experienced reduced levels of mechanical stress [40]. Z-directed PEMFs induced further cytoplasmic redistribution of YAP in MSCs on the RND scaffolds, reflected as a reduction in YAP nuclear/cytoplasm ratio, whereas X-directed PEMFs had no significant effect on YAP

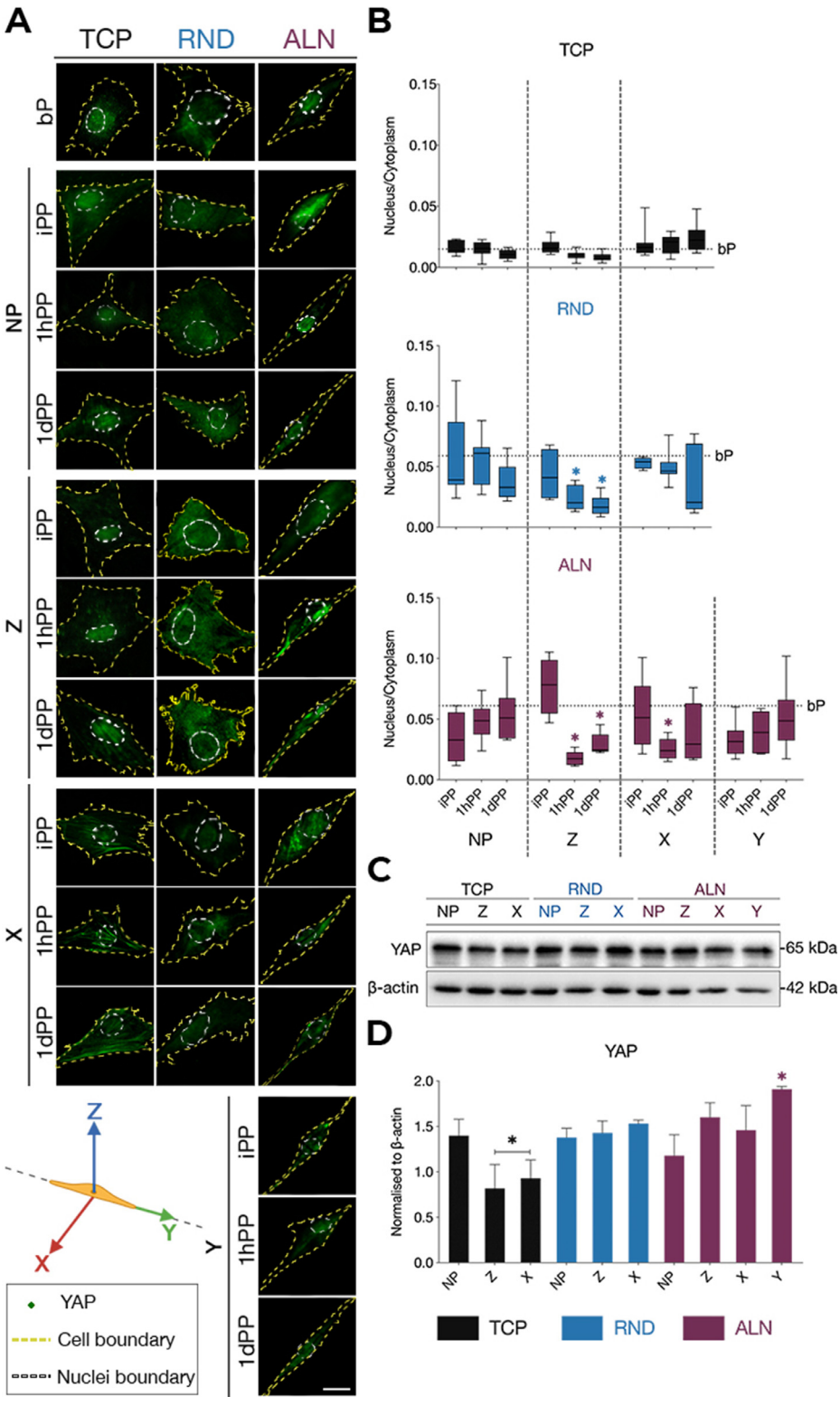

Fig. 6. Effects of directional PEMFs on YAP localisation and expression in MSCs laden on TCP, RND and ALN. **(A)** YAP probing by IFS (green ≡ YAP; yellow dashes ≡ cell boundary; white dashes ≡ nuclei boundary). Scale bar represents 10 μm and applies to all images. **(B)** Semi-quantification of YAP localisation presented as nucleus/cytoplasm ratio. Data shown represent means ± SD, n = 15. **(C)** Western blot analysis of total YAP in MSCs harvested 1-hour post-pulse, where the bar graph represents the quantification of the total YAP protein at 1hPP. Data shown represent means ± SD, n = 3 from 3 independent experiments. * denotes significance compared to the non-exposed group of the respective topography ($p < 0.05$). Z, X and Y coordinates represent PEMF exposure direction; NP denotes no PEMFs.

localisation (Fig. 6B). Analogously, cytoplasmic redistribution of YAP was observed in MSCs on ALN scaffolds in response to both Z-directed and X-directed, whereas Y-directed PEMFs had no effect. PEMF exposure did not alter YAP localization in MSCs on TCP. Total YAP protein levels were reduced by Z- and X-directed PEMFs in MSCs on TCP but were unaffected in MSCs on RND and ALN scaffolds. Uniquely, Y-directed PEMFs augmented total YAP levels in MSCs on ALN scaffolds (Fig. 6C). Therefore, a cytoplasmic YAP localisation correlated with chondrogenic induction by Z-directed PEMFs on RND scaffolds and signs of reduced mechanotransduction signalling.

3.8. Role of pFAK in transducing PEMF effect on MSC chondrogenesis

Inhibition of FAK phosphorylation confirmed the role of pFAK in transducing the effects of directional PEMFs on MSC chondrogenesis within the RND scaffolds. The pFAK inhibitor, PF573228 (pFAKi), suppressed FAK phosphorylation in response to both Z- and X-directed PEMFs to below the basal levels (Fig. 7A) as well as suppressed the enhancement in ERK phosphorylation induced by Z-directed PEMFs (Fig. 7B). Notably, there were no significant changes in the basal (0 mT) pFAK/FAK or pERK/ERK ratios following pFAK inhibition. Inhibition of FAK phosphorylation in itself was permissive for chondrogenesis under all conditions with reference to *ACAN* and *COL II* expression, and was further accentuated by PEMF exposure, particularly when exposed to X-directed PEMFs (Fig. 7C). The transcriptional enhancement of ECM proteins detected upon pFAK inhibition was corroborated at the protein, showing a reversal of the suppression of COL II deposition by X-directed PEMF exposure to levels similar to those induced by Z-directed PEMFs (Fig. 7D-E). pFAK inhibition is thus capable of reversing the chondrogenic suppression induced by X-directed PEMFs.

3.9. Effects of directional PEMFs on mitochondrial stress and the role of pFAK

Prior reports have shown that analogous PEMFs exert developmental consequences by modulating mitochondrial function [24,31]. We therefore examined the interplay between field directionality and mitochondrial respiration in MSCs on the RND scaffolds. Mitochondrial oxygen consumption rate (OCR) was generally enhanced by PEMF exposure. Notably, X-directed PEMF exposure induced much greater increases in spare respiratory capacity and maximal respiration than Z-directed PEMF exposure (Fig. 8), whereas, the application of FAK inhibitor, applied only during PEMF exposure, suppressed both spare respiratory capacity and maximal respiration to similar levels. Basal respiration and ATP-coupled oxygen consumption rates were induced and inhibited by Z- and X-directed PEMFs, respectively, yet were strongly inhibited by FAK inhibition across the board. Finally, non-ATP-coupled OCR was uniquely increased by the Z-directed PEMFs but was strongly suppressed pFAK inhibition in all conditions.

4. Discussion

Existing studies examining the capacity of PEMF-based strategies to promote MSC chondrogenesis have generated conflicting results. Notable discrepancies surround the duration and frequency of exposure, where cumulative exposure is commonly in the order of hours over the course of a few weeks [26,41,42]. We have previously demonstrated that overexposure to PEMFs was developmentally counterproductive [23,24,31], and brief exposure to PEMFs (10 minutes), applied once, were most efficacious at promoting MSC chondrogenesis in pellet cultures [23]. Imperative to the described unique efficacy was the timing of PEMF exposure to coincide with the developmental expression of TRPC1 channels [23,24,31], which limited our window for PEMF exposure to the period of early chondrogenic induction and is specific to our unique exposure paradigm [23]. We have also previously found that sensitivity to our PEMFs was modulated by the extracellular mechanical environment [43]. The combination of these parameters define our exposure paradigm and distinguishe it from other published protocols. In this report, we extended our investigation of potential starting conditions with which to increase responsiveness to PEMFs by examining the interplay between magnetic field orientation, cell alignment and basal mechanotransduction.

The distinct substrates compared in this study established diverse micromechanical cellular environments. MSCs on TCP and the ALN scaffolds displayed morphologies and cytoskeletal arrangements characteristic of cells experiencing axial mechanical tension, polygonal or fibroblastic, respectively (Fig. 2B, G), and were associated with nuclear YAP localisation (Fig. 6A). Notably, MSCs on ALN scaffolds were bipolarly aligned along the long axis of the scaffolds, whereas MSCs on TCP were multipolar (Fig. 2G). By contrast, MSCs on the RND scaffolds were spherically-symmetrical and exhibited predominantly cytoplasmic YAP localisation.

MSCs with rounded morphologies are associated with greater chondrogenic potential [44,45], coinciding with evidence that low levels of cytoskeleton tension are more permissive for chondrogenesis [46,47] and arise from the sum of all cytoskeleton-substrate interactions [48]. Focal adhesion complexes were smaller, more numerous and evenly distributed in MSCs on the RND scaffolds (Fig. 5B), reflecting a greater number of substrate attachments of relatively lesser force. Despite FAK activation being required for MSC fate determination [49,50], MSC condensation leading to chondrogenesis [51] is favoured by transient FAK activation [52]. On the other hand, sustained cytoskeletal traction forces favouring nuclear YAP translocation [21] are associated with inhibition of MSC chondrogenesis [22]. It thus appears that the heightened chondrogenic potential conferred by the RND scaffolds is a consequence of their propensity to create low mechanical force environments.

Both RND and ALN fibrous scaffolds have previously been demonstrated to be conducive for MSC chondrogenesis [53,54], with ALN fibres biasing differentiation towards a fibrocartilage phenotype [29,30], seemingly contradicting with the current study demonstrating heightened COL I formation on the RND scaffolds (Fig. 4C). The discrepancy might be due to the greater compliance of the elastomeric sub-nano-sized PLCL fibres used in the present study. Nonetheless, the RND and ALN scaffolds offered an opportunity to investigate the interactions of distinct mechanical environments with magenetic field directionality. Chondrogenic enhancement was greatest for MSCs impregnated onto the RND scaffolds exposed to Z-directed PEMFs (Fig. 4) and was associated with suppressions in the *COL I/COL II* and *COL X/COL II* ratios, indicating the promotion of hyaline cartilage. By contrast, PEMFs did not promote chondrogenic differentiation of MSCs on either TCP or the ALN scaffolds, irrespective of field directionality. It thus appears that the lower levels of resting tension afforded by the RND scaffolds (Fig. 5B) provided the best mechanical environment with which Z-directed PEMFs to promote MSC-chondrogenesis chondrogenesis.

PEMFs administered parallel to the plane of the tissue culture dish, in either the X or Y directions, attenuated cell proliferation on either nanofibrous scaffold (Fig. 3E). Viability of MSCs was not affected by magnetic field direction on the RND scaffolds (Fig. 3D), whereas the incidence of MSC apoptosis was increased and decreased by "*parallel*" PEMFs on TCP and the ALN scaffolds, respectively (Fig. 3D); Z-directed ("*orthogonal*") PEMF exposure of MSCs on the ALN scaffolds exhibited similar levels of viability as their respective RND counterparts. Taken together, the absence of PEMF-induced MSC chondrogenesis in response to "*parallel*" PEMFs on

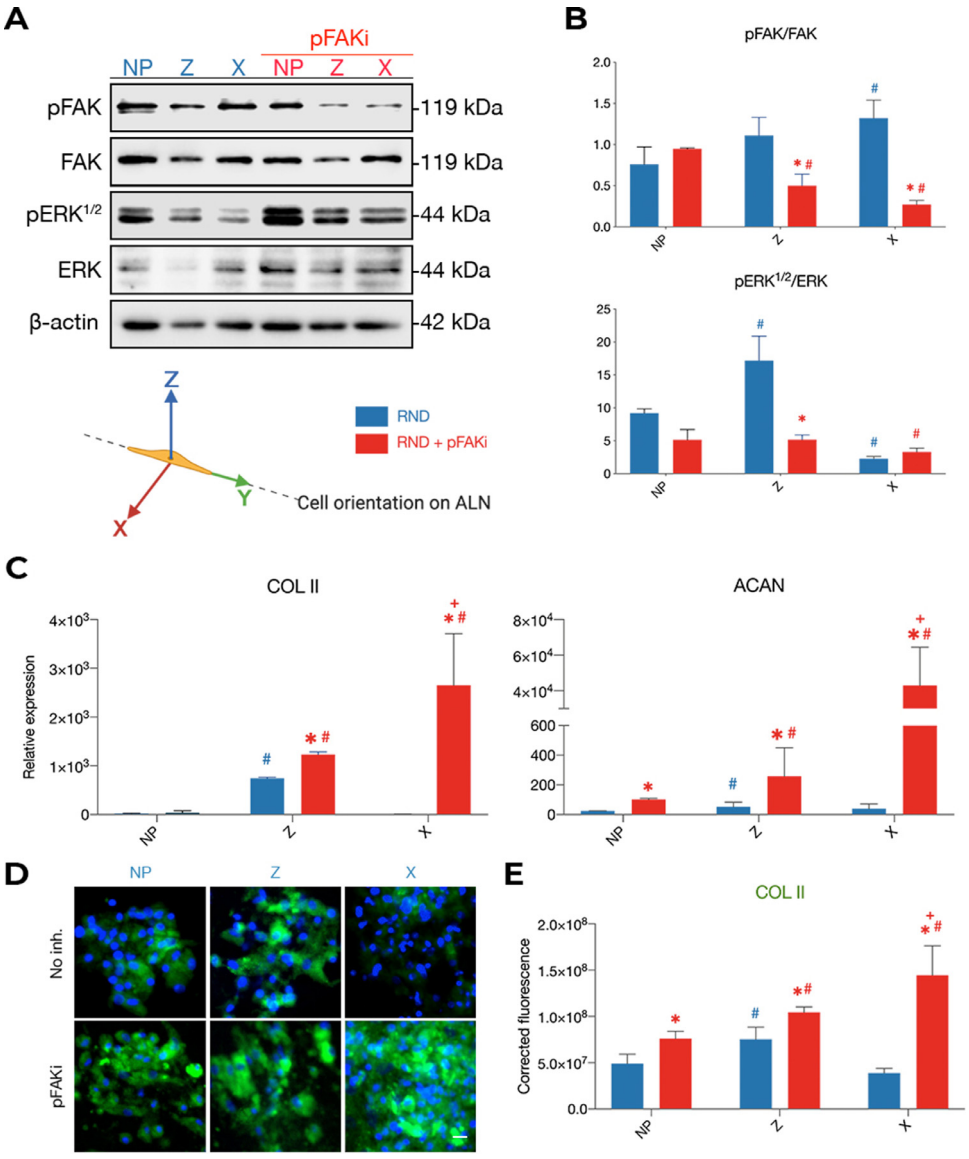

Fig. 7. Role of pFAK signalling in transducing PEMF effect to MSC chondrogenesis on RND fibrous scaffolds. **(A)** Western blot analysis of FAK and ERK protein phosphorylation measured 1-hour following PEMF exposure in the presence (red bars) or absence (blue bars) of FAK inhibitor. **(B)** Semi-quantification of pFAK and pERK protein levels. Data shown represent means ± SD, n = 3 from 3 independent experiments. **(C)** Expression of *COL II* and *ACAN* by PEMF-treated MSCs in the presence (red bars) or absence of FAK inhibitor (blue bars). Data shown represent means ± SD, n = 6 from 2 independent experiments. **(D)** Immunofluorescent staining for COL II deposition in response to PEMFs at Day 21 of differentiation. Scale bar represents 20 μm and applies to all groups. **(E)** Semi-quantification of COL II by IFS. Data shown represent means ± SD, n = 15. * denotes significance levels compared to the non-inhibited group in each treatment. # denotes significance compared to the non-exposed, non-inhibited control group, whereas + denotes significance levels comparing X to Z ($p < 0.05$). Z, X and Y coordinates represent PEMF exposure direction; NP denotes no PEMFs.

the RND and ALN scaffolds cannot be attributed to compromised cell viability.

Agreeing with our previous report examining PEMF-induced MSC chondrogenesis in pellet cultures [23], a single 10-min exposure administered at the start of differentiation induction was more chondrogenically effective than longer or repeated exposures (Fig. 3B-C). Here we add a further level of specificity by showing that MSCs on the RND scaffolds were more sensitive to magnetic exposure, responding best at 1 mT, rather than 2 mT for MSC pellet cultures [23], in response to PEMFs of the same orientation (Z-directed). Accordingly, we previously demonstrated that the culturing microenvironment modulates the PEMF sensitivity of MSCs undergoing chondrogenesis [43]. These different mechanical microenvironments likely elicited distinct mechanotransduction responses, ultimately influencing MSC responses to magnetic field stimulation by impinging upon a common second messenger signalling cascades yet, via magnetic and mechanical transduction events. The outcome of the combined responses of substrate-based mechanical input with field orientation would hence be cumulative and synergistic.

MSC chondrogenesis is best promoted by transient activation of FAK [52], whereas its sustained activation impedes chondrogenesis [11,50]. Z-directed PEMFs applied to the RND scaffolds, reduced pFAK (Fig. 5C), enhanced cytoplasmic redistribution of YAP (Fig. 6B), increased ERK phosphorylation (Fig. 5F-G) and, accordingly, enhanced chondrogenesis. By direct contrast, X-directed PEMFs applied to the RND scaffolds increased FAK activation, decreased ERK phosphorylation (Fig. 6G), produced no detectable change in YAP localisation (Fig. 6B) and inhibited MSC chondrogenesis. Since neither the macroscopic mechanical environment nor amplitude of the magnetic fields differ in the distinct orientations, differences in cell sheet spreading in the horizontal (plane of the

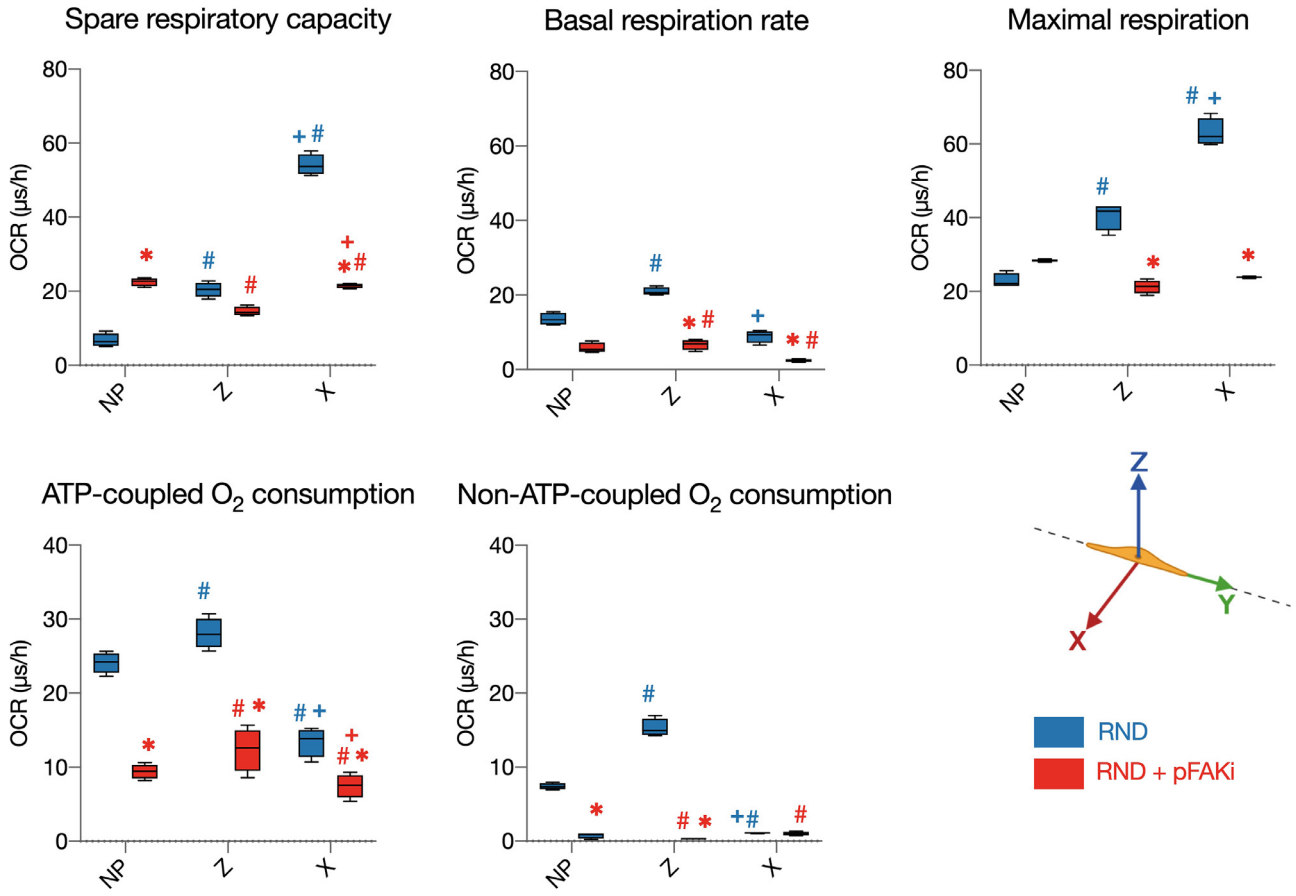

Fig. 8. Role of inhibition of FAK (red bars) on cellular respiration on the RND scaffolds. Data shown represent means ± SD, n = 6 from 2 independent experiments. * denotes significance levels compared to the non-inhibited group (blue bars) in each treatment. # denotes significance compared to the non-exposed, non-inhibited control group, whereas + denotes significance levels comparing X to Z ($p < 0.05$). Z, X and Y coordinates represent PEMF exposure direction; NP denotes no PEMFs.

dish) and vertical planes are the most likely variable to account for the detected difference (Fig. 1B). These results reveal an interplay between magnetic field directionality and the mechanical preconditioning conferred by fibrous scaffolds, mediated via cytoskeleton dynamics involving the FAK/ERK/YAP signalling axis.

4.1. Mitochondrial interplay between mechanotransduction and magnetoreception

We have previously demonstrated that PEMFs induce calcium entry through transient receptor potential (TRPC1) channels [24], promoting both *in vitro* chondrogenesis [23] and myogenesis [31] by activating a calcium-dependent mitochondrial-transcriptional axis. On one level, TRPC1 function has previously been linked to both cellular mechanotransduction [55] and magnetoreception [23,31], which, in turn, would influence cytoskeletal remodelling and associated mechanotransduction [56]. On another level, mitochondrial activation and the production of reactive oxygen species (ROS) has been reported for both TRPC1-mediated magnetoreception [24,31] and mechanotransduction [57,58]. It is thus consistend with available evidence that mechanotransduction and magnetoreception interact via a mutual impingement upon mitochondrial respiration. Here, we show that PEMF directionality differentially modulates mitochondrial respiration in MSCs undergoing chondrogenesis. Z-directed PEMFs applied to MSCs on the RND scaffolds moderately stimulated basal respiration that correlated with enhanced chondrogenic outcome, whereas X-directed PEMFs produced more exaggerated increases respiratory capacities (Fig. 8) that instead coincided with compromised chondrogenic induction (Fig. 4A). Subtle differences in ROS levels have been shown to have disparate effects on MSC-derived chondogenesis [57–59]. For instance, whereas NADPH oxidases-generated ROS are indispensable for survival and deposition of sGAG in the early-stage of chondrogenesis [60,61], excessive ROS have been shown to promote hypertrophic switching during chondrocyte differentiation [62,63]. Hence, the exaggerated level of oxygen consumption, the prime source of mitochondrial ROS, produced by X-directed PEMF exposure likely stymied chondrogenic progression and accounted for the hypertrophy development (Fig. 8). Excessive ROS production also has been shown to inhibit phosphatases implicated in the MAPK cascades [64], thereby accounting for the reduction in ERK activation we observed by X-directed PEMFs (Fig. 5F-G). Notably, FAK inhibition effectively normalised mitochondrial respiratory differences between all conditions to below basal levels, indicating that FAK is activated under all conditions, including the unexposed, contributed to calpain-dependend proteolytic modulation of FAK downstream of TRPC1-mediated calcium entry [65], possibly modulated by both ambient and supplemental magnetic fields [31].

TRPC1 is activated by ROS [66] and conversely, TRPC1-mediated calcium entry stimulates mitochondrial ROS, revealing a system of mutual reinforcement [31]. Cellular mechanotransduction may hence set the redox background whereupon magnetic fields subsequently act to regulate MSC differentiation via a process described as magnetic mitohormesis [31]. FAK staining indicates that resting cytoskeletal tensions of MSCs are least on the RND scaffolds and highest on TCP (Fig. 5B, D-E). Accepting that PEMF exposure and resting mechanotransduction act cumulatively in a mitohormetic

fashion, increases and decreases (excessive mitochondrial activation) in FAK phosphorylation in response to magnetic exposure of fixed amplitude substantiates pre-existing low and high levels of resting mechanical tension, respectively, correspondent to X-directed PEMFs applied to MSCs on the RND scaffolds and Z-directed PEMFs applied to MSCs on TCP (Fig. 5D-E). It must be stipulated, however, that these results are cumulative, representing the combined mitochondrial responses of cytoskeletal-based mechanotransduction in conjunction with those induced by magnetic fields, both impinging on TRPC1. Therefore, within a wider mitohormetic context sensitivity to PEMF directionality and amplitude is likely to differ depending on the nature of the micromechanical environment and should be accounted for when designing magnetic exposure paradigms for tissue engineering means.

4.2. Influence of magnetic field directionality

Previous studies have demonstrated an anisotropic relationship between magnetic field direction and induced mitochondrial respiration [67]. Having shown that similar PEMFs to those employed in present study induce mitochondrial respiration in other progenitor cell classes [24,31], we examined the contribution of field alignment over mitochondrial responses in MSCs undergoing chondrogenic induction. At the quantum biological level, it has been shown that Z- and X-directed electromagnetic fields disparately modulate mitochondrial respiration [67]. We also demonstrate an interaction between magnetic field directionality and cell orientation, an effect that was best revealed by employing the ALN scaffolds. Any such effect would have been averaged out in MSCs impregnated onto the RND scaffolds or TCP. At the level of cellular alignment, it was previously calculated that magnetic fields perpendicular to the long axis of cylindrically modelled cells would have a greater effect on induced ion motion, such as that for calcium, at the cell surface than fields parallel to the long axis of said cells that would translate into differences in cell response [68]. Our reported responses with reference to magnetic field directionality hence reflect a combination of these two biophysical properties of magnetic fields over cellular mitochondrial responses. Here, we presented two cell scenarios where field directionality was either *orthogonal* or *parallel* to general cell alignment and associated with relative maxima and minima: **1**) cells plated in 2D in the X-Y plane in response to Z-directed fields and; **2**) Y-aligned cells exposed to Y-directed fields, respectively, in accordance with this proposed mechanism.

5. Conclusion

Chondrogenic responses to PEMF exposure were modulated by both micromechanical environment as well as the degree of cross-alignment of cells with the fields. Our results indicate that the efficacy of PEMF-induced MSC chondrogenesis is regulated in a multifaceted manner involving focal adhesion dynamics, cytoskeleton remodelling, as well as mitochondrial responses that will ultimately need to be taken into consideration when developing future tissue engineering platforms aimed at magnetically-assisted MSC-derived chondrogenesis.

Authors' contributions

CC conducted all experimental work, data acquisition and analyses, interpretation of data as well as the manuscript writing. AF-O provided the PEMF device and expertise, interpreted data and participated in manuscript writing. EHL acquired the funding and reviewed the manuscript. ZY acquired funding, designed, interpreted data and contributed to the manuscript writing. All authors reviewed the final manuscript.

Declaration of Competing Interest

AF-O is an inventor on patent WO 2019/17863 A1, System and Method for Applying Pulsed Electromagnetic Fields, wherein field directionality effects are described, as well as, a founder of QuantumTx Pte Ltd, which elaborates electromagnetic field devices for human use. The other authors declare no conflicts of interest.

Acknowledgements

This work was supported by funding from Singapore Ministry of Education (MOE2019-T2-1-127). CC was supported by SINGA Scholarship, A*STAR.

Supplementary materials

Supplementary material associated with this article can be found, in the online version, at doi:10.1016/j.actbio.2020.10.039.

References

[1] M. Pumberger, T.H. Qazi, M.C. Ehrentraut, M. Textor, J. Kueper, G. Stoltenburg-Didinger, T. Winkler, P. von Roth, S. Reinke, C. Borselli, C. Perka, D.J. Mooney, G.N. Duda, S. Geissler, Synthetic niche to modulate regenerative potential of MSCs and enhance skeletal muscle regeneration, Biomaterials 99 (2016) 95–108 https://doi.org/10.1016/j.biomaterials.2016.05.009.
[2] G. Chamberlain, J. Fox, B. Ashton, J. Middleton, Concise Review, Mesenchymal Stem Cells: Their Phenotype, Differentiation Capacity, Immunological Features, and Potential for Homing, Stem Cells 25 (2007) 2739–2749 https://doi.org/10.1634/stemcells.2007-0197.
[3] H. Afizah, J.H. Hui, Mesenchymal stem cell therapy for osteoarthritis, J Clin Orthop Trauma 7 (2016) 177–182 https://doi.org/10.1016/j.jcot.2016.06.006.
[4] K. Pelttari, E. Steck, W. Richter, The use of mesenchymal stem cells for chondrogenesis, Inj. Int J Care Inj 39S1 (2008) S58–S65 https://doi.org/10.1016/j.injury.2008.01.038.
[5] H. Nejadnik, J.H. Hui, E.P. Feng Choong, B.C. Tai, E.H. Lee, Autologous bone marrow-derived mesenchymal stem cells versus autologous chondrocyte implantation: an observational cohort study, Am J Sports Med 38 (2010) 1110–1116 https://doi.org/10.1177/0363546509359067.
[6] M. Lo Monaco, G. Merckx, J. Ratajczak, P. Gervois, P. Hilkens, P. Clegg, A. Bronckaers, J.M. Vandeweerd, I. Lambrichts, Stem Cells for Cartilage Repair: Preclinical Studies and Insights in Translational Animal Models and Outcome Measures, Stem Cells Int (2018) 1–22 2018 https://doi.org/10.1155/2018/9079538 .
[7] S. Wakitani, K. Imoto, T. Yamamoto, M. Saito, N. Murata, M. Yoneda, Human autologous culture expanded bone marrow mesenchymal cell transplantation for repair of cartilage defects in osteoarthritic knees, Osteoarthritis Cartilage 10 (2002) 199–206 https://doi.org/10.1053/joca.2001.0504.
[8] Z. Ge, C. Li, B. Heng, G. Cao, Z. Yang, Functional biomaterials for cartilage regeneration, J Biomed Mater Res A 100 (2012) 2526–2536.
[9] C. O'Conor, N. Case, F. Guliak, Mechanical regulation of chondrogenesis, Stem Cell Res Ther 4 (2013) 6.
[10] D. Discher, D. Mooney, P. Zandstra, Growth factors, matrices, and forces combine and control stem cells, Science 324 (2009) 1673–1677.
[11] T. Zhang, F. Wen, Y. Wu, G.S. Goh, Z. Ge, L.P. Tan, J.H. Hui, Z. Yang, Cross-talk between TGF-beta/SMAD and integrin signaling pathways in regulating hypertrophy of mesenchymal stem cell chondrogenesis under deferral dynamic compression, Biomaterials 38 (2015) 72–85 https://doi.org/10.1016/j.biomaterials.2014.10.010.
[12] Y.N. Wu, J.B. Law, A.Y. He, H.Y. Low, J.H. Hui, C.T. Lim, Z. Yang, E.H. Lee, Substrate topography determines the fate of chondrogenesis from human mesenchymal stem cells resulting in specific cartilage phenotype formation, Nanomed 10 (2014) 1507–1516 https://doi.org/10.1016/j.nano.2014.04.002.
[13] Y. Wu, Z. Yang, J.B.K. Law, A.Y. He, A.A. Abbas, V. Denslin, T. Kamarul, J.H.P. Hui, E.H. Lee, The Combined Effect of Substrate Stiffness and Surface Topography on Chondrogenic Differentiation of Mesenchymal Stem Cells, Tissue Eng. Part A. 23 (2017) 43–54 https://doi.org/10.1089/ten.tea.2016.0123.
[14] B. Geiger, A. Bershadsky, R. Pankov, K.M. Yamada, Transmembrane extracellular matrix-cytoskeleton crosstalk, Nat Rev Mol Cell Biol 2 (2001) 793–805.
[15] Y. Tang, R.G. Rowe, E.L. Botvinick, A. Kurup, A.J. Putnam, M. Seiki, V.M. Weaver, E.T. Keller, S. Goldstein, J. Dai, D. Begun, T. Saunders, S.J. Weiss, MT1-MMP-dependent control of skeletal stem cell commitment via a beta1-integrin/YAP/TAZ signaling axis, Dev Cell 25 (2013) 402–416 https://doi.org/10.1016/j.devcel.2013.04.011.
[16] X. He, H. Wang, T. Jin, Y. Xu, L. Mei, J. Yang, TLR4 Activation Promotes Bone Marrow MSC Proliferation and Osteogenic Differentiation via Wnt3a and Wnt5a Signaling, PLoS One 11 (2016) e0149876 https://doi.org/10.1371/journal.pone.0149876.
[17] M. Kuroda, H. Wada, Y. Kimura, K. Ueda, N. Kioka, Vinculin promotes nuclear localization of TAZ to inhibit ECM stiffness-dependent differentiation into adipocytes, J Cell Sci 130 (2017) 989–1002 https://doi.org/10.1242/jcs.194779.

[18] Q. Chen, M.S. Kinch, T.H. Lin, K. Burridge, R.L. Juliano, Integrin-mediated cell adhesion activates mitogen-activated protein kinases, J. Biol. Chem. 269 (1994) 26602–26605.
[19] S. Dupont, L. Morsut, M. Aragona, E. Enzo, S. Giulitti, M. Cordenonsi, F. Zanconato, J. Le Digabel, M. Forcato, S. Bicciato, N. Elvassore, S. Piccolo, Role of YAP/TAZ in mechanotransduction, Nature 474 (2011) 179–183 https://doi.org/10.1038/nature10137.
[20] S. Dupont, Role of YAP/TAZ in cell-matrix adhesion-mediated signalling and mechanotransduction, Exp Cell Res 343 (2016) 42–53 https://doi.org/10.1016/j.yexcr.2015.10.034.
[21] W. Zhong, Y. Li, L. Li, W. Zhang, S. Wang, X. Zheng, YAP-mediated regulation of the chondrogenic phenotype in response to matrix elasticity, J Mol Histol 44 (2013) 587–595 https://doi.org/10.1007/s10735-013-9502-y.
[22] A. Karystinou, A.J. Roelofs, A. Neve, F.P. Cantatore, H. Wackerhage, C. De Bari, Yes-associated protein (YAP) is a negative regulator of chondrogenesis in mesenchymal stem cells, Arthritis Res Ther 17 (2015) 1–14 https://doi.org/10.1186/s13075-015-0639-9.
[23] D. Parate, A. Franco-Obregon, J. Frohlich, C. Beyer, A.A. Abbas, T. Kamarul, J.H.P. Hui, Z. Yang, Enhancement of mesenchymal stem cell chondrogenesis with short-term low intensity pulsed electromagnetic fields, Sci Rep 7 (2017) 9421 https://doi.org/10.1038/s41598-017-09892-w.
[24] F. Kurth, Y.K. Tai, D. Parate, M. van Oostrum, Y.R.F. Schmid, S.J. Toh, J.L. Yee Yap, B. Wollscheid, A. Othman, P.S. Dittrich, A. Franco-Obregón, Cell-Derived Vesicles as TRPC1 Channel Delivery Systems for the Recovery of Cellular Respiratory and Proliferative Capacities, Adv Biosys (2020) https://doi.org/10.1101/2020.05.16.099283.
[25] Y.K. Tai, C. Ng, K. Purnamawati, J.L.Y. Yap, J.N. Yin, C. Wong, B.K. Patel, P.L. Soong, P. Pelczar, J. Fröhlich, C. Beyer, C.H.H. Fong, S. Ramanan, M. Casarosa, C.P. Cerrato, Z.L. Foo, R.M. Pannir Selvan, E. Grishina, U. Degirmenci, S.J. Toh, P.J. Richards, A. Mirsaidi, K. Wuertz-Kozak, S.Y. Chong, S.J. Ferguson, A. Aguzzi, M. Monici, L. Sun, C.L. Drum, J. Wang, A. Franco-Obregón, Magnetic fields modulate metabolism and gut microbiome in correlation with *Pgc-1α*; expression: Follow-up to an in vitro magnetic mitohormetic study, FASEB J 34 (2020) 11143–11167 https://doi.org/10.1096/fj.201903005RR.
[26] M. Esposito, A. Lucariello, C. Costanzo, A. Fiumarella, A. Giannini, G. Riccardi, I. Riccio, Differentiation of human umbilical cord-derived mesenchymal stem cells, WJ-MSCs, into chondrogenic cells in the presence of pulsed electromagnetic fields, In Vivo 27 (2013) 495–500.
[27] J. Huang, Y. Liang, Z. Huang, P. Zhao, Q. Liang, Y. Liu, L. Duan, W. Liu, F. Zhu, L. Bian, J. Xia, J. Xiong, D. Wang, Magnetic Enhancement of Chondrogenic Differentiation of Mesenchymal Stem Cells, ACS Biomater. Sci. Eng. 5 (2019) 2200–2207 https://doi.org/10.1021/acsbiomaterials.9b00025.
[28] C.L. Ross, M. Siriwardane, G. Almeida-Porada, C.D. Porada, P. Brink, G.J. Christ, B.S. Harrison, The effect of low-frequency electromagnetic field on human bone marrow stem/progenitor cell differentiation, Stem Cell Res 15 (2015) 96–108 https://doi.org/10.1016/j.scr.2015.04.009.
[29] W. Zhong, W. Zhang, S. Wang, J. Qin, Regulation of fibrochondrogenesis of mesenchymal stem cells in an integrated microfluidic platform embedded with biomimetic nanofibrous scaffolds, PLoS One 8 (2013) e61283 https://doi.org/10.1371/journal.pone.0061283.
[30] W.M. Han, S.J. Heo, T.P. Driscoll, M.E. Boggs, R.L. Duncan, R.L. Mauck, D.M. Elliot, Impact of cellular microenvironment and mechanical perturbation on calcium signalling in meniscus fibrochondrocytes, Eur Cell Mater 27 (2015) 321–331.
[31] J.L.Y. Yap, Y.K. Tai, J. Fröhlich, C.H.H. Fong, J.N. Yin, Z.L. Foo, S. Ramanan, C. Beyer, S.J. Toh, M. Casarosa, N. Bharathy, M.P. Kala, M. Egli, R. Taneja, C.N. Lee, A. Franco-Obregón, Ambient and supplemental magnetic fields promote myogenesis via a TRPC1-mitochondrial axis: evidence of a magnetic mitohormetic mechanism, FASEB J 33 (2019) 12853–12872 https://doi.org/10.1096/fj.201900057R.
[32] S. Crocetti, C. Beyer, G. Schade, M. Egli, J. Frohlich, A. Franco-Obregon, Low intensity and frequency pulsed electromagnetic fields selectively impair breast cancer cell viability, PLoS One 8 (2013) e72944 https://doi.org/10.1371/journal.pone.0072944.
[33] M.E. Berginski, S.M. Gomez, The Focal Adhesion Analysis Server: a web tool for analyzing focal adhesion dynamics, F1000Res 2 (2013) 68 https://doi.org/10.12688/f1000research.2-68.v1.
[34] D.R. Hipfner, S.M. Cohen, Connecting proliferation and apoptosis in development and disease, Nat. Rev. Mol. Cell Biol. 5 (2004) 805–815 https://doi.org/10.1038/nrm1491.
[35] N.A. Arita, D. Pelaez, H.S. Cheung, Activation of the extracellular signal-regulated kinases 1 and 2 (ERK1/2) is needed for the TGFbeta-induced chondrogenic and osteogenic differentiation of mesenchymal stem cells, Biochem Biophys Res Commun 405 (2011) 564–569 https://doi.org/10.1016/j.bbrc.2011.01.068.
[36] P.P. Provenzano, D.R. Inman, K.W. Eliceiri, P.J. Keely, Matrix density-induced mechanoregulation of breast cell phenotype, signaling and gene expression through a FAK-ERK linkage, Oncogene 28 (2009) 4326–4343 https://doi.org/10.1038/onc.2009.299.
[37] S. Wan, X. Fu, Y. Ji, M. Li, X. Shi, Y. Wang, FAK- and YAP/TAZ dependent mechanotransduction pathways are required for enhanced immunomodulatory properties of adipose-derived mesenchymal stem cells induced by aligned fibrous scaffolds, Biomaterials 171 (2018) 107–117 https://doi.org/10.1016/j.biomaterials.2018.04.035.
[38] T.P. Driscoll, B.D. Cosgrove, S.J. Heo, Z.E. Shurden, R.L. Mauck, Cytoskeletal to Nuclear Strain Transfer Regulates YAP Signaling in Mesenchymal Stem Cells, Biophys J 108 (2015) 2783–2793 https://doi.org/10.1016/j.bpj.2015.05.010.
[39] S. Piccolo, S. Dupont, M. Cordenonsi, The biology of YAP/TAZ: hippo signaling and beyond, Physiol Rev. 94 (2014) 1287–1312 https://doi.org/10.1152/physrev.00005.2014.
[40] M. Fischer, P. Rikeit, P. Knaus, C. Coirault, YAP-Mediated Mechanotransduction in Skeletal Muscle, Front. Physiol. 7 (2016) 1–12 https://doi.org/10.3389/fphys.2016.00041.
[41] H. Kavand, N. Haghighipour, B. Zeynali, E. Seyedjafari, B. Abdemami, Extremely Low Frequency Electromagnetic Field in Mesenchymal Stem Cells Gene Regulation: Chondrogenic Markers Evaluation, Artif Organs 40 (2016) 929–937 https://doi.org/10.1111/aor.12696.
[42] S. Mayer-Wagner, A. Passberger, B. Sievers, J. Aigner, B. Summer, T.S. Schiergens, V. Jansson, P.E. Muller, Effects of low frequency electromagnetic fields on the chondrogenic differentiation of human mesenchymal stem cells, Bioelectromagnetics 32 (2011) 283–290 https://doi.org/10.1002/bem.20633.
[43] D. Parate, N.D. Kadir, C. Celik, E.H. Lee, J.H.P. Hui, A. Franco-Obregón, Z. Yang, Pulsed electromagnetic fields potentiate the paracrine function of mesenchymal stem cells for cartilage regeneration, Stem Cell Res. Ther. 11 (2020) 1–16 https://doi.org/10.1186/s13287-020-1566-5.
[44] S. Zhou, S. Chen, Q. Jiang, M. Pei, Determinants of stem cell lineage differentiation toward chondrogenesis versus adipogenesis, Cell Mol Life Sci 76 (2019) 1653–1680 https://doi.org/10.1007/s00018-019-03017-4.
[45] S. Ichinose, M. Tagami, T. Muneta, I. Sekiya, Morphological examination during in vitro cartilage formation by human mesenchymal stem cells, Cell Tissue Res 322 (2005) 217–226 https://doi.org/10.1007/s00441-005-1140-6.
[46] S. Ghosh, M. Laha, S. Mondal, S. Sengupta, D.L. Kaplan, In vitro model of mesenchymal condensation during chondrogenic development, Biomaterials 30 (2009) 6530–6540 https://doi.org/10.1016/j.biomaterials.2009.08.019.
[47] J.S. Park, J.S. Chu, A.D. Tsou, R. Diop, Z. Tang, A. Wang, S. Li, The effect of matrix stiffness on the differentiation of mesenchymal stem cells in response to TGF-beta, Biomaterials 32 (2011) 3921–3930 https://doi.org/10.1016/j.biomaterials.2011.02.019.
[48] A. Woods, G. Wang, F. Beier, Regulation of chondrocyte differentiation by the actin cytoskeleton and adhesive interactions, J Cell Physiol 213 (2007) 1–8 https://doi.org/10.1002/jcp.21110.
[49] S.K. Mitra, D.A. Hanson, D.D. Schlaepfer, Focal adhesion kinase: in command and control of cell motility, Nat Rev Mol Cell Biol 6 (2005) 56–68 https://doi.org/10.1038/nrm1549.
[50] I. Takahashi, Effect of stretching on gene expression of beta1 integrin and focal adhesion kinase and on chondrogenesis through cell-extracellular matrix interactions, Eur. J. Cell Biol. 82 (2003) 182–192 https://doi.org/10.1078/0171-9335-00307.
[51] A.M. Delise, R.S. Tuan, Analysis of N-cadherin function in limb mesenchymal chondrogenesis in vitro, Dev Dyn 225 (2002) 195–204 https://doi.org/10.1002/dvdy.10151.
[52] O.S. Bang, E.J. Kim, J.G. Chung, S.R. Lee, T.K. Park, S.S. Kang, Association of focal adhesion kinase with fibronectin and paxillin is required for precartilage condensation of chick mesenchymal cells, Biochem Biophys Res Commun 278 (2000) 522–529 https://doi.org/10.1006/bbrc.2000.3831.
[53] J.K. Wise, A.L. Yarin, C.M. Megaridis, M. Cho, Chondrogenic differentiation of human mesenchymal stem cells on oriented nanofibrous scaffolds: engineering the superficial zone of articular cartilage, Tissue Eng. Part A. 15 (2009) 913–921.
[54] Y.Y. Li, T.H. Choy, F.C. Ho, P.B. Chan, Scaffold composition affects cytoskeleton organization, cell-matrix interaction and the cellular fate of human mesenchymal stem cells upon chondrogenic differentiation, Biomaterials 52 (2015) 208–220 https://doi.org/10.1016/j.biomaterials.2015.02.037.
[55] A. Patel, R. Sharif-Naeini, J.R.H. Folgering, D. Bichet, F. Duprat, E. Honoré, Canonical TRP channels and mechanotransduction: from physiology to disease states, Pflüg. Arch. - Eur. J. Physiol. 460 (2010) 571–581 https://doi.org/10.1007/s00424-010-0847-8.
[56] J. Canales, D. Morales, C. Blanco, J. Rivas, N. Díaz, I. Angelopoulos, O. Cerda, A TR(i)P to Cell Migration: New Roles of TRP Channels in Mechanotransduction and Cancer, Front. Physiol. 10 (2019) 757 https://doi.org/10.3389/fphys.2019.00757.
[57] M.F. Forni, J. Peloggia, K. Trudeau, O. Shirihai, A.J. Kowaltowski, Murine Mesenchymal Stem Cell Commitment to Differentiation Is Regulated by Mitochondrial Dynamics, Stem Cells 34 (2016) 743–755 https://doi.org/10.1002/stem.2248.
[58] K.V. Tormos, E. Anso, R.B. Hamanaka, J. Eisenbart, J. Joseph, B. Kalyanaraman, N.S. Chandel, Mitochondrial complex III ROS regulate adipocyte differentiation, Cell Metab 14 (2011) 537–544 https://doi.org/10.1016/j.cmet.2011.08.007.
[59] T. Finkel, Signal transduction by reactive oxygen species, J Cell Biol 194 (2011) 7–15 https://doi.org/10.1083/jcb.201102095.
[60] K. Morita, T. Miyamoto, N. Fujita, Y. Kubota, K. Ito, K. Takubo, K. Miyamoto, K. Ninomiya, T. Suzuki, R. Iwasaki, M. Yagi, H. Takaishi, Y. Toyama, T. Suda, Reactive oxygen species induce chondrocyte hypertrophy in endochondral ossification, J. Exp. Med. 204 (2007) 1613–1623 https://doi.org/10.1084/jem.20062525.
[61] K.S. Kim, H.W. Choi, H.E. Yoon, I.Y. Kim, Reactive Oxygen Species Generated by NADPH Oxidase 2 and 4 Are Required for Chondrogenic Differentiation, J. Biol. Chem. 285 (2010) 40294–40302 https://doi.org/10.1074/jbc.M110.126821.
[62] A. Maziarz, B. Kocan, M. Bester, S. Budzik, M. Cholewa, T. Ochiya, A. Banas, How electromagnetic fields can influence adult stem cells: positive and

negative impacts, Stem Cell Res Ther 7 (2016) 1–12 https://doi.org/10.1186/s13287-016-0312-5.
[63] K.J. Wolff, P.S. Ramakrishnan, M.J. Brouillette, B.J. Journot, T.O. McKinley, J.A. Buckwalter, J.A. Martin, Mechanical stress and ATP synthesis are coupled by mitochondrial oxidants in articular cartilage, J Orthop Res 31 (2013) 191–196 https://doi.org/10.1002/jor.22223.
[64] K. Lee, W.J. Esselman, Inhibition of PTPs by H2O2 regulates the activation of distinct MAPK pathways, Free Radic. Biol. Med. 33 (2002) 1121–1132.
[65] M. Louis, N. Zanou, M. Van Schoor, P. Gailly, TRPC1 regulates skeletal myoblast migration and differentiation, J. Cell Sci. 121 (2008) 3951–3959 https://doi.org/10.1242/jcs.037218.
[66] O.L. Gervasio, N.P. Whitehead, E.W. Yeung, W.D. Phillips, D.G. Allen, TRPC1 binds to caveolin-3 and is regulated by Src kinase - role in Duchenne muscular dystrophy, J. Cell Sci 121 (2008) 2246–2255 https://doi.org/10.1242/jcs.032003.
[67] R.J. Usselman, C. Chavarriaga, P.R. Castello, M. Procopio, T. Ritz, E.A. Dratz, D.J. Singel, C.F. Martino, The Quantum Biology of Reactive Oxygen Species Partitioning Impacts Cellular Bioenergetics, Sci. Rep. 6 (2016) 38543 https://doi.org/10.1038/srep38543.
[68] C. Polk, Physical mechanisms by which low-frequency magnetic fields can affect the distribution of counterions on cylindrical biological cell surfaces, J. Biol. Phys. 14 (1986) 3–8 https://doi.org/10.1007/BF01857978.